

Landau levels of Majorana fermions in a spin liquid

Stephan Rachel,¹ Lars Fritz,² and Matthias Vojta¹

¹*Institut für Theoretische Physik, Technische Universität Dresden, 01062 Dresden, Germany*

²*Institute for Theoretical Physics and Center for Extreme Matter and Emergent Phenomena, Utrecht University, Leuvenlaan 4, 3584 CE Utrecht, The Netherlands*

(Dated: Sep 2, 2015)

Majorana fermions were originally proposed as elementary particles acting as their own antiparticles¹. In recent years, it has become clear that Majorana fermions can instead be realized in condensed-matter systems as emergent quasiparticles, a situation often accompanied by topological order². Here we propose a physical system which realizes Landau levels – highly degenerate single-particle states usually resulting from an orbital magnetic field acting on charged particles – for Majorana fermions. This is achieved in a variant of a quantum spin system due to Kitaev³ which is distorted by triaxial strain. This strained Kitaev model displays a spin-liquid phase with charge-neutral Majorana-fermion excitations whose spectrum corresponds to that of Landau levels, here arising from a tailored pseudo-magnetic field⁴. We show that measuring the dynamic spin susceptibility reveals the Landau-level structure by a remarkable mechanism of probe-induced bound-state formation.

In 1937 E. Majorana suggested¹ that a real wavefunction can describe spin-1/2 quantum particles that are their own antiparticles. Consequently, these particles are charge-neutral and decouple from the electromagnetic field, making them hard to detect. While no observation of Majorana fermions as elementary particles has been reported to date, their possible realization as emergent quasiparticles in condensed-matter systems has attracted enormous attention. Specifically, it was realized that superconductors provide a natural habitat, where Bogoliubov quasiparticles at zero energy have properties of Majorana fermions². Moreover, a seminal work of Kitaev³ demonstrated that dispersive Majorana fermions can emerge as effective degrees of freedom in spin-liquid phases of frustrated quantum magnets⁵. This has triggered an intense search for materials which come close to realizing Kitaev’s spin-liquid model on the honeycomb lattice, with A₂IrO₃ (A=Na, Li) currently being the best candidates^{6–8}.

Here we show that the properties of emergent Majorana fermions in quantum magnets can be engineered by controlled lattice distortions. We use spatially inhomogeneous magnetic couplings, generated by applying a suitable strain pattern, to transform the linear Dirac-like dispersion of low-energy Majorana fermions in the Kitaev model into a sequence of pseudo-Landau levels. The idea of strain-induced Landau levels was in fact first theoretically proposed⁴ and then subsequently realized⁹ for elec-

trons in two-dimensional graphene. Our work adapts this concept to the charge-neutral fractionalized quasiparticles of a topological spin liquid. We compute the dynamic spin susceptibility which turns out to display sharp excitations at isolated energies reflecting the Landau-level structure of the strained spin liquid.

Model

The Kitaev model³ describes quantum spins 1/2 on a honeycomb lattice subject to spin-anisotropic Ising (or “compass”) interactions. The Hamiltonian, generalized to spatially varying couplings, reads

$$\mathcal{H}_K = - \sum_{\langle ij \rangle_x} J_{ij}^x \hat{\sigma}_i^x \hat{\sigma}_j^x - \sum_{\langle ij \rangle_y} J_{ij}^y \hat{\sigma}_i^y \hat{\sigma}_j^y - \sum_{\langle ij \rangle_z} J_{ij}^z \hat{\sigma}_i^z \hat{\sigma}_j^z \quad (1)$$

where $\hat{\sigma}^\alpha$ are Pauli matrices, and $\langle ij \rangle_\alpha$ denotes an α bond as shown in Fig. 1, with $\alpha = x, y, z$. This model displays an infinite set of constants of motion, which can be interpreted as \mathbb{Z}_2 fluxes through the closed loops of the lattice. Upon representing each spin $\hat{\sigma}$ by four Majorana fermions $\hat{b}^x, \hat{b}^y, \hat{b}^z$ and \hat{c} , with $\hat{\sigma}_i^\alpha = i \hat{b}_i^\alpha \hat{c}_i$, the model (1) takes the form

$$\mathcal{H}_{\hat{a}} = \frac{i}{2} \sum_{\langle ij \rangle} J_{ij}^\alpha \hat{u}_{ij} \hat{c}_i \hat{c}_j, \quad (2)$$

where $\hat{u}_{ij} \equiv i \hat{b}_i^{\alpha ij} \hat{b}_j^{\alpha ij}$ and $\hat{u}_{ij} = -\hat{u}_{ji}$. The operators \hat{u}_{ij} represent conserved quantities with eigenvalues of $u_{ij} = \pm 1$ which determine the values of the \mathbb{Z}_2 fluxes. Hence the Hamiltonian $\mathcal{H}_{\hat{a}}$ (2) represents a nearest-neighbor hopping problem for the c (or “matter”) Majorana fermions which are coupled to a static \mathbb{Z}_2 gauge field. Its exact solution can be written in terms of canonical-fermion excitation modes with non-negative energies ϵ_m , for details see methods. For homogeneous and isotropic couplings, $J_{ij}^\alpha \equiv J$, it describes a \mathbb{Z}_2 spin liquid with matter-fermion excitations displaying a gapless Dirac spectrum.

Majorana Landau levels

In the context of graphene, it has been theoretically shown⁴ that a suitable spatial modulation of hopping energies can mimic the effect of an orbital magnetic field in

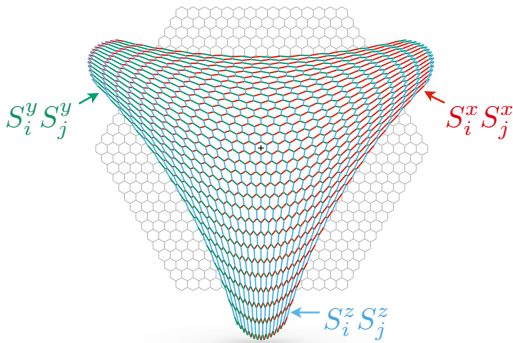


FIG. 1: Honeycomb-lattice flake with $N = 675$ unit cells where bonds with different color correspond to Ising interactions J^α of different spin components α . The distorted lattice visualizes the displacement according to Eq. (3) arising from triaxial strain; the unstrained hexagonal flake is shown in the back in grey. Longer (shorter) bonds correspond to weaker (stronger) exchange couplings J_{ij}^α .

Dirac electron systems. At low energies, the modulation can be represented as pseudo-magnetic field, with opposite sign for electrons belonging to the two Dirac cones (or “valleys”) located at $\vec{K} = (4\pi/(3\sqrt{3}), 0)$ and $\vec{K}' = (-4\pi/(3\sqrt{3}), 0)$ (with the lattice constant a_0 set to unity), such that time-reversal symmetry is preserved. If this pseudo-magnetic field is sufficiently homogeneous – applying e.g. to triaxial strain patterns as shown in Fig. 1 – it can induce single-particle pseudo-Landau levels very similar to Landau levels in a physical magnetic field. The system then displays a so-called quantum valley Hall effect⁴, *i.e.*, it combines a chiral and an antichiral quantum Hall effect at the valleys \vec{K} and \vec{K}' , respectively. For triaxial strain the displacement vector is given by^{4,10}

$$\vec{U}(x, y) = \bar{C}(2xy, x^2 - y^2) \quad (3)$$

where \bar{C} (measured in units of $1/a_0$) parameterizes the distortion. This displacement yields – to first order in \bar{C} – a homogeneous pseudo-magnetic field whose strength is proportional to \bar{C} .

Adapting the idea of strain-induced artificial gauge fields to spin systems, we study the Kitaev model (1) with spatially modulated exchange couplings. Given that the Majorana-fermion hopping matrix elements in Eq. (2) are given by the exchange couplings J_{ij}^α , we choose

$$J_{ij}^\alpha = J^\alpha \left[1 - \beta(|\vec{\delta}_{ij}|/a_0 - 1) \right] \quad (4)$$

where we calculate the distance $\vec{\delta}_{ij} = \vec{R}_i + \vec{U}_i - \vec{R}_j - \vec{U}_j$ using the $\vec{U}(x, y)$ from Eq. (3) evaluated at the lattice positions \vec{R}_i of the undistorted honeycomb lattice. The factor β encodes the strength of magnetoelastic coupling, and the parameter (dubbed “strain” below) $C = \bar{C}\beta$ will enter our simulations as a measure of the modulations of the J_{ij}^α . We note that, for a real material, Eq. (4)

represents a linear approximation to the full dependence of the exchange constant on the bond length¹⁰.

The inhomogeneous Kitaev model (1) with couplings given by Eq. (4) is expected to display a \mathbb{Z}_2 spin-liquid phase with an extremely unusual excitation spectrum: While the \mathbb{Z}_2 fluxes remain static, the matter Majorana fermions will form highly degenerate Landau levels.

This is well borne out by our numerical results, obtained for finite-size Kitaev systems of hexagonal shape, Fig. 1, with open zigzag boundaries and lattice sizes up to $2N = 15\,000$ sites. We focus on the case of isotropic couplings and choose $J^\alpha = J$ as energy unit. Provided that the strain C is not too large, the ground state is located in the flux-free sector where all u_{ij} can be chosen to be +1. We monitor the local density of states (LDOS) of the matter fermions¹¹ which is shown in the top panels of Fig. 2: While this is the familiar honeycomb-lattice DOS in the unstrained case $C = 0$ [panel (a)], with $\rho(\omega) \propto \omega$ at low energies, the results for finite strain show clear Landau-level peaks at low energies highlighted by the black arrows in panels (d) and (g). In particular, the Landau-level energies ε_n display the scaling $\varepsilon_n \propto \sqrt{nC}$ with the lowest Landau level (LLL) located at zero energy, characteristic of honeycomb-lattice Dirac fermions.

In order to detect the Landau-level structure, we propose to measure dynamic spin correlations

$$S_{ij}^{\alpha\beta}(t) = \langle \hat{\sigma}_i^\alpha(t) \hat{\sigma}_j^\beta(0) \rangle \quad (5)$$

whose Fourier transform is – in a magnet – accessible by neutron scattering experiments. We restrict our attention to zero temperature where $S_{ij}^{\alpha\beta}(\omega)$ is proportional to the imaginary part of the dynamic spin susceptibility. The evaluation of the dynamic spin correlations in the Kitaev model has been first discussed in Ref. 12. Specifically, the application of the operator $\hat{\sigma}_i^\alpha = i \hat{b}_i^\alpha \hat{c}_i$ changes the \mathbb{Z}_2 fluxes in the plaquettes adjacent to the α bond emanating from site i . Starting from the ground state $|0\rangle$ which is flux-free, the intermediate state $|\lambda\rangle$ is then a state with a locally excited flux pair, *i.e.*, the hopping problem of matter fermions in the intermediate state involves a local “flux impurity” $\hat{V} = -2i J_{ij}^\alpha \hat{c}_i \hat{c}_j$.

Applied to the strained Kitaev model, a central observation is that the impurity \hat{V} induces a sequence of single-particle bound states which energetically lie between the Landau levels. This can be nicely seen in panels (e) and (h) of Fig. 2 which show the LDOS in the two-flux sector, measured on the flipped bond. This LDOS displays essentially the same Landau levels as the corresponding flux-free system, but shows additional sharp peaks of even higher weight at energies E_n in between the Landau levels – these peaks arise from isolated states localized near the flipped bond. We note that related bound states have been reported recently in a study of spin excitations in the field-induced non-Abelian phase of the Kitaev model¹³. More broadly, recent theory work on topological band insulators has suggested that the generic occurrence of impurity-induced bound states in

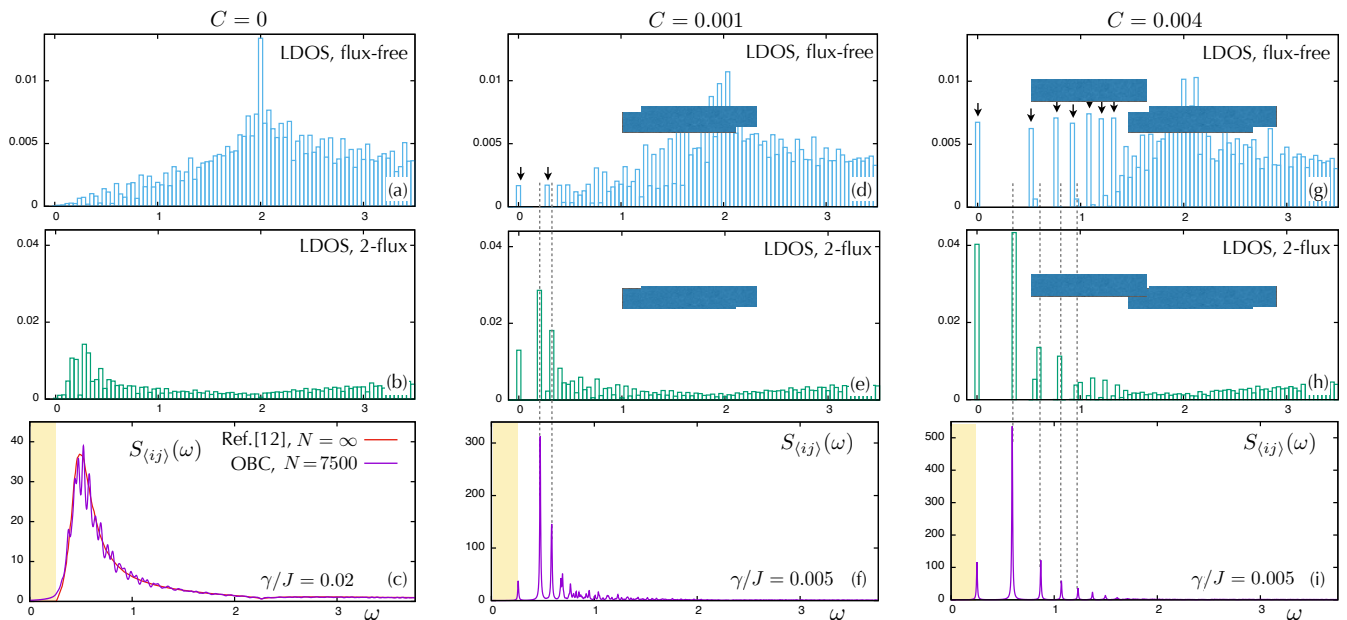


FIG. 2: Histogram of the matter-fermion LDOS in the flux-free (top, blue) and two-flux sectors (middle, green), together with the dynamical spin correlator $S_{\langle ij \rangle}(\omega)$ with $S_{\langle ij \rangle} = S_{ii} + S_{jj} + 2S_{ij}$ (bottom, purple), for the cases (a-c): unstrained ($C = 0$), (d-f): moderate strain ($C = 1 \cdot 10^{-3}$), and (g-i): large strain ($C = 4 \cdot 10^{-3}$). All quantities are measured in the center of a sample with $2N = 15000$ sites. The $S(\omega)$ plots employ a Lorentzian broadening of width γ ; moreover the energy axis has been shifted with respect to the LDOS plots by the amount of the local flux gap Δ_{ij} ¹¹ (yellow region). Panel (c) also shows $S(\omega)$ for the infinite homogeneous system¹². While the LDOS of the flux-free sector [panel (d) and (g)] nicely shows the emergence of Majorana Landau levels (black arrows), the two-flux sector features bound states in the gaps between the Landau levels [panels (e) and (h)] – these are detected in $S_{\langle ij \rangle}(\omega)$ as sharp peaks (dashed lines are guide-to-the-eye).

a two-dimensional gapped system is a signature of its topological nature¹⁴. For the present case of bond impurities in the triaxially strained honeycomb lattice, we have checked that bound states between the Landau levels occur indeed generically, i.e., independent of the impurity strength¹¹, hinting at the topological character of the matter-fermion sector.

Remarkably, these Majorana-fermion bound states enable a unique detection of the Landau-level structure: The largest matrix elements for the correlator $S_{\langle ij \rangle}(\omega)$ arise from these bound states in the two-flux sector, such that $S_{\langle ij \rangle}(\omega)$ displays sharp peaks at $E_n + \Delta_{ij}$ where Δ_{ij} is the local flux gap^{11,15}. As can be seen in the lower panels of Fig. 2, these bound-state peaks dominate over the peaks arising from the Landau levels themselves. Given that sharp bound states can only arise in gapped systems, the sequence of peaks in $S_{\langle ij \rangle}(\omega)$ represents a direct signature of the peculiar excitation spectrum – Landau levels separated by gaps – of the strained spin liquid.

Discussion

Our results raise a number of further issues. First, we note that the simultaneous application of strain and of a physical magnetic field has non-trivial effects, which can be analyzed perturbatively by projecting onto the flux-

free sector³. We have found that the LLL of the strained Kitaev model is shifted to a finite energy, while otherwise the spectrum of the matter Majorana fermions remains qualitatively unchanged. The excitations of the now fully gapped system obey non-Abelian statistics similar to the elementary excitations of Kitaev’s B-phase³ subject to a magnetic field. Second, and perhaps most interesting, is the fate of the Landau-level spin liquid when interactions beyond the Kitaev model are included¹⁶. While this question is beyond the scope of this work, it is likely that the large degeneracy of the many-body ground state will be lifted in favor of potentially exotic states driven by interactions between the Majorana fermions, akin to the physics of the fractional quantum Hall effect.

Realizations of our system appear possible using strained thin films of honeycomb-lattice iridates, where it has been proposed that homogeneous pressure or strain may drive the material into a Kitaev spin-liquid regime. Landau levels can then be generated using shapes resulting from triaxial strain, circular arcs¹⁷, or nanobubbles⁹. A second possibility is offered by advances in designing artificial molecular structures on surfaces, where the electronic structure of strained graphene has already been demonstrated¹⁸. A third option is by simulating the Hamiltonian (1) using ultracold atomic gases. Phase plates¹⁹ or digital mirror devices²⁰ can be used to directly project the distorted lattice onto a 2D cloud of atoms,

and proposals for realizing artificial spin-orbit coupling have been made²¹.

In summary, we have demonstrated how to engineer a novel state of matter, where the emergent degrees of freedom of a fractionalized spin liquid – charge-neutral Majorana fermions – display a Landau-level structure of excitation energies. We have shown that this Landau-level structure can be efficiently detected in measurements of dynamic spin correlations, thanks to a mechanism of probe-induced bound-state formation.

Methods

The Kitaev model (1) is equivalent to the following bilinear Hamiltonian for the matter Majorana fermions

$$\mathcal{H}_u = \frac{i}{2} (\hat{c}_A^T \hat{c}_B^T) \begin{pmatrix} 0 & M \\ -M^T & 0 \end{pmatrix} \begin{pmatrix} \hat{c}_A \\ \hat{c}_B \end{pmatrix} \quad (6)$$

where M is an $N \times N$ matrix with elements $M_{ij} = J_{ij}^\alpha u_{ij}$ and $\hat{c}_{A(B)}$ is a vector of length N of Majorana operators on the $A(B)$ sublattice. We construct the matrix M for

couplings given by Eq. (4) and diagonalize the problem via a singular-value decomposition which yields the excitation energies and the eigenmodes. From these we calculate the LDOS as the local spectral density of the c fermions.

The calculation of a zero-temperature dynamic structure factor $S_{ij}(\omega)$ involves two diagonalizations, one in the flux-free sector with all $u = 1$ and one in the excited-state flux sector with all $u = 1$ except $u_{ij} = -1$ on the bond involving the measured site(s). The eigenvectors in both flux sectors are then used to construct the matrix elements entering the dynamic structure factor. Details are given in the supplement.

Acknowledgments

We thank J. Knolle, T. Meng, M. Neek-Amal, F. Peeters, and F. Zschöcke for discussions. This research was supported by the DFG through SFB 1143 and GRK 1621 as well as by the Helmholtz association through VI-521.

-
- ¹ E. Majorana, Teoria simmetrica dell'elettrone e del positrone, *Nuovo Cimento* **14**, 171-184 (1937). English translation: A symmetric theory of electrons and positrons, *Soryushiron Kenkyu* **63**, 149-162 (1981).
- ² C. W. J. Beenakker, Search for Majorana fermions in superconductors, *Annu. Rev. Con. Mat. Phys.* **4**, 113 (2013).
- ³ A. Kitaev, Anyons in an exactly solved model and beyond, *Ann. Phys. (N.Y.)* **321**, 2-111 (2006).
- ⁴ F. Guinea, M. I. Katsnelson, and A. K. Geim, Energy gaps and a zero-field quantum Hall effect in graphene by strain engineering, *Nature Phys.* **6**, 30 (2009).
- ⁵ L. Balents, Spin liquids in frustrated magnets, *Nature* **464**, 199 (2010).
- ⁶ J. Chaloupka, G. Jackeli, and G. Khaliullin, Kitaev-Heisenberg Model on a Honeycomb Lattice: Possible Exotic Phases in Iridium Oxides A_2IrO_3 , *Phys. Rev. Lett.* **105**, 027204 (2010).
- ⁷ Y. Singh *et al.*, Relevance of the Heisenberg-Kitaev Model for the Honeycomb Lattice Iridates A_2IrO_3 , *Phys. Rev. Lett.* **108**, 127203 (2012).
- ⁸ S. H. Chun *et al.*, Direct evidence for dominant bond-directional interactions in a honeycomb lattice iridate Na_2IrO_3 , *Nature Phys.* **11**, 462 (2015).
- ⁹ N. Levy *et al.*, Strain-Induced Pseudo-Magnetic Fields greater than 300 Tesla in Graphene nanobubbles, *Science* **329**, 544 (2010).
- ¹⁰ M. Neek-Amal, L. Covaci, K. Shakouri, and F. M. Peeters, Electronic structure of a hexagonal graphene flake subjected to triaxial stress, *Phys. Rev. B* **88**, 115428 (2013).
- ¹¹ See supplemental material.
- ¹² J. Knolle, D. L. Kovrizhin, J. T. Chalker, and R. Moessner, Dynamics of a two-dimensional quantum spin liquid: signatures of emergent Majorana fermions and fluxes, *Phys. Rev. Lett.* **112**, 207203 (2014).
- ¹³ J. Knolle, D. L. Kovrizhin, J. T. Chalker, and R. Moessner, Dynamics of Fractionalization in Quantum Spin Liquids, preprint arXiv:1507.02865.
- ¹⁴ R.-J. Slager, L. Rademaker, J. Zaanen, and L. Balents, Impurity Bound States and Greens Function Zeroes as Local Signatures of Topology, *Phys. Rev. B* **92**, 085126 (2015).
- ¹⁵ F. Zschöcke and M. Vojta, Physical states and finite-size effects in Kitaev's honeycomb model: Bond disorder, spin excitations, and NMR lineshape, *Phys. Rev. B* **92**, 014403 (2015).
- ¹⁶ M. Hermanns, S. Trebst, and A. Rosch, Spin-Peierls Instability of Three-Dimensional Spin Liquids with Majorana Fermi Surfaces, preprint arXiv:1506.01379.
- ¹⁷ F. Guinea, A. K. Geim, M. I. Katsnelson, and K. S. Novoselov, Generating quantizing pseudomagnetic fields by bending graphene ribbons, *Phys. Rev. B* **81**, 035408 (2010).
- ¹⁸ K. K. Gomes, W. Mar, W. Ko, F. Guinea, and H. C. Manoharan, Designer Dirac fermions and topological phases in molecular graphene, *Nature* **483**, 306 (2012).
- ¹⁹ W. S. Bakr, J. Gillen, A. Peng, S. Fölling, and M. Greiner, A quantum gas microscope for detecting single atoms in a Hubbard-regime optical lattice, *Nature* **462**, 74 (2009).
- ²⁰ C. Muldoon *et al.*, Control and manipulation of cold atoms in optical tweezers, *New J. Phys.* **14**, 073051 (2012).
- ²¹ J. Dalibard, F. Gerbier, G. Juzeliūnas, and P. Öhberg, *Colloquium: Artificial gauge potentials for neutral atoms*, *Rev. Mod. Phys.* **83**, 1523 (2011).

Supplemental material: Landau levels of Majorana fermions in a spin liquid

Stephan Rachel,¹ Lars Fritz,² and Matthias Vojtá¹

¹*Institut für Theoretische Physik, Technische Universität Dresden, 01062 Dresden, Germany*

²*Institute for Theoretical Physics and Center for Extreme Matter and Emergent Phenomena,
Utrecht University, Leuvenlaan 4, 3584 CE Utrecht, The Netherlands*

(Dated: Sep 2, 2015)

I. EXACT SOLUTION OF THE KITAEV MODEL

The spin-liquid model of Kitaev¹ describes spins 1/2 on a honeycomb lattice which interact via bond-dependent nearest-neighbor Ising spin exchange,

$$\mathcal{H}_K = - \sum_{\langle ij \rangle_x} J_{ij}^x \hat{\sigma}_i^x \hat{\sigma}_j^x - \sum_{\langle ij \rangle_y} J_{ij}^y \hat{\sigma}_i^y \hat{\sigma}_j^y - \sum_{\langle ij \rangle_z} J_{ij}^z \hat{\sigma}_i^z \hat{\sigma}_j^z \quad (\text{S1})$$

with $\hat{\sigma}_i^\alpha$ being Pauli matrices. For the homogeneous isotropic case, $J_{ij}^\alpha \equiv J$, the Kitaev model possesses a discrete \mathbb{Z}_3 symmetry of a combination of 120 degree real-space and simultaneous spin rotations of the form $\hat{\sigma}^x \rightarrow \hat{\sigma}^y$, $\hat{\sigma}^y \rightarrow \hat{\sigma}^z$, and $\hat{\sigma}^z \rightarrow \hat{\sigma}^x$. As usual, the two sublattices of the honeycomb lattice will be labelled A and B.

Following Kitaev¹ one rewrites the spin Hamiltonian (S1) in terms of four Majorana fermions per site, \hat{b}^x , \hat{b}^y , \hat{b}^z , and \hat{c} , with $\hat{\sigma}_i^\alpha = i\hat{b}_i^\alpha \hat{c}_i$. In the new operators, the Hamiltonian (S1) becomes

$$\mathcal{H}_{\hat{u}} = \frac{i}{2} \sum_{\langle ij \rangle_\alpha} J_{ij}^\alpha \hat{u}_{ij} \hat{c}_i \hat{c}_j \quad (\text{S2})$$

with the ‘‘bond operator’’ $\hat{u}_{ij} \equiv i\hat{b}_i^\alpha \hat{b}_j^\alpha$ which is antisymmetric under exchange of i and j (and i taken from the A sublattice). The problem can be solved by noting that all \hat{u}_{ij} are constants of motion: they commute with the Hamiltonian $\mathcal{H}_{\hat{u}}$ and with each other, their eigenvalues being $u_{ij} = \pm 1$. Every particular choice of a given set $\{u_{ij}\}$ reduces the Hamiltonian (S2) into a bilinear which is readily solved,

$$\mathcal{H}_u = \frac{i}{2} \begin{pmatrix} \hat{c}_A^T & \hat{c}_B^T \end{pmatrix} \begin{pmatrix} 0 & M \\ -M^T & 0 \end{pmatrix} \begin{pmatrix} \hat{c}_A \\ \hat{c}_B \end{pmatrix}. \quad (\text{S3})$$

For a honeycomb lattice with $2N$ lattice sites, M is a real $N \times N$ matrix with elements $M_{jk} = J_{jk}^\alpha u_{jk}$ and the vector $\hat{c}_{A(B)}$ contains N matter Majorana operators of the A (B) sublattice. Using a singular value decomposition one finds $M = USV^T$ with orthogonal $N \times N$ matrices U and V and the positive semi-definite diagonal matrix S with elements ϵ_i , $i = 1, \dots, N$. Denoting the Majorana fermions on sublattice A (B) in unit cell \mathbf{r} as $\hat{c}_{A(B),\mathbf{r}}$, the Majorana eigenmodes are given by

$$\hat{c}'_{A,m} = \sum_{\mathbf{r}} U_{m,\mathbf{r}}^T \hat{c}_{A,\mathbf{r}} \quad \text{and} \quad \hat{c}'_{B,m} = \sum_{\mathbf{r}} V_{m,\mathbf{r}}^T \hat{c}_{B,\mathbf{r}} \quad (\text{S4})$$

which can be combined into complex fermions

$$\hat{a}_m = \frac{1}{2} (\hat{c}'_{A,m} + i\hat{c}'_{B,m}). \quad (\text{S5})$$

Using the matrix identity

$$\begin{pmatrix} 0 & USV^T \\ -VSU^T & 0 \end{pmatrix} = \begin{pmatrix} U & 0 \\ 0 & V \end{pmatrix} \begin{pmatrix} 0 & S \\ -S & 0 \end{pmatrix} \begin{pmatrix} U^T & 0 \\ 0 & V^T \end{pmatrix} \quad (\text{S6})$$

we can rewrite the Hamiltonian (S3),

$$\begin{aligned} \mathcal{H}_u &= \frac{i}{2} \begin{pmatrix} \hat{c}_A^T & \hat{c}_B^T \end{pmatrix} \begin{pmatrix} U & 0 \\ 0 & V \end{pmatrix} \begin{pmatrix} 0 & S \\ -S & 0 \end{pmatrix} \begin{pmatrix} U^T & 0 \\ 0 & V^T \end{pmatrix} \begin{pmatrix} \hat{c}_A \\ \hat{c}_B \end{pmatrix} \\ &= \frac{i}{2} (\hat{c}'_A{}^T \hat{c}'_B{}^T) \begin{pmatrix} 0 & S \\ -S & 0 \end{pmatrix} \begin{pmatrix} \hat{c}'_A \\ \hat{c}'_B \end{pmatrix} \\ &= i \sum_{m=1}^N \epsilon_m \hat{c}'_{A,m} \hat{c}'_{B,m} = \sum_{m=1}^N \epsilon_m (2\hat{a}_m^\dagger \hat{a}_m - 1). \quad (\text{S7}) \end{aligned}$$

The matter-fermion excitation energies are thus given by the singular values ϵ_m of the matrix M ; the ground-state energy for a given choice of $\{u_{ij}\}$ is $E_{0,u} = -\sum_m \epsilon_m$. Following Kitaev we will refer from now on to the choices $\{u_{ij}\}$ as flux sectors. The case where all $u_{ij} = +1$ is referred to as the *flux-free* sector. The case where all $u_{ij} = +1$ except a single $u_{\mu\nu} = -1$ is referred to as a *single-flux sector* if the bond $\langle \mu\nu \rangle$ is located at the boundary of the sample and as *two-flux sector* otherwise.

To monitor the eigenmodes of the matter Majorana fermions, we can calculate their (global) density of states (DOS), $\rho(\omega) = \sum_n \delta(\omega - 2\epsilon_n)$. To resolve spatial structure, we also consider the corresponding local density of states (LDOS) which is given by

$$\rho_j(\omega) = \frac{1}{2} \sum_n U_{nj}^2 \delta(\omega - 2\epsilon_n) \quad (\text{S8})$$

for a site j on the A sublattice; for a site j on the B sublattice, U_{nj} is replaced by V_{nj} where U_{nj} (V_{nj}) are the matrix elements of U (V).

In our numerical calculations we consider hexagonal flakes with open boundaries (see Fig. S1), consisting of r rings, with the number of unit cells being $N = 3r^2$. Most runs are performed for $r = 50$, yielding $2N = 15000$ spins.

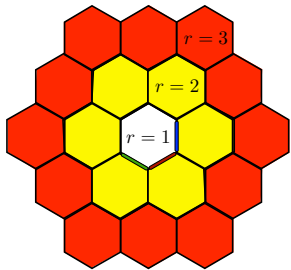


FIG. S1: Illustration of a hexagonal shaped honeycomb flake consisting of r “rings”. Shown are $r = 1$ (white), $r = 2$ (yellow + white), $r = 3$ (red + yellow + white). The number of unit cells is $N = 3r^2$ corresponding to $2N$ spins.

II. DYNAMICAL SPIN CORRELATIONS

The dynamical spin correlation function, Eq. (5) of the main paper, can be expressed in terms of Majorana fermions and yield the following Lehmann representation at zero temperature^{2,3}, here written separately for the on-site correlator

$$S_{ii}^{\alpha\beta}(\omega) = 2\pi \sum_{\lambda} | \langle M_0 | \hat{c}_i | \lambda \rangle |^2 \delta(\omega - (E_{\lambda} - E_0)) \delta_{\alpha\beta} \quad (\text{S9})$$

and the off-site correlators

$$S_{ij}^{\alpha\beta}(\omega) = 2\pi F_{ij}^{\alpha} \sum_{\lambda} \langle M_0 | \hat{c}_i | \lambda \rangle \langle \lambda | \hat{c}_j | M_0 \rangle \times \delta(\omega - (E_{\lambda} - E_0)) \delta_{\alpha\beta} \delta_{\langle ij \rangle \alpha}, \quad (\text{S10})$$

where $\delta_{\langle ij \rangle \alpha}$ is non-zero only if i and j are nearest neighbors connected by an α bond, i.e., S_{ij} vanishes beyond nearest neighbors. In both cases $|M_0\rangle$ is the matter-fermion ground state in the ground-state flux sector, assumed to be flux-free, and \sum_{λ} runs over all matter-fermion states in the two-flux sector. E_0 and E_{λ} are the corresponding many-body energies. The prefactor $F_{ij}^{\alpha} = \{-1, i, -i\}$ depending on the spin component. Note that we can safely ignore the fermion parity condition^{3,4} due to open boundaries, such that $|M_0\rangle$ has no excited matter fermions. For the intermediate state $|\lambda\rangle$ we will restrict ourselves to states with a single matter fermion; these states contribute more than 97% of the spectral weight in the homogeneous case².

In the homogeneous isotropic Kitaev model, the momentum-dependent dynamic spin structure factor $S^{\alpha\alpha}(\vec{q}, \omega) = (1/N) \sum_{ij} S_{ij}^{\alpha\alpha}(\omega) e^{-i\vec{q}\cdot\vec{r}_{ij}}$ – accessible by neutron scattering – displays a continuum of spectral weight above the energy of the flux gap, $\Delta = 0.26J$, with little momentum dependence². This reflects the fact that a spin flip decays into a matter and a flux excitation, the latter having a momentum-independent energy.

For our inhomogeneous Kitaev model, the computation of the spin correlator proceeds in the following steps:

1. We construct the matrix M in (S6) for the flux-free sector (i.e., all $u_{ij} = +1$). This matrix is real and of dimension $N \times N$, its entries require to specify the values of J^{α} and the strain C .
2. We perform a singular value decomposition (SVD) into $M = USV^T$ where U and V contain the normalized singular vectors and are orthogonal, $U^T = U^{-1}$ and $V^T = V^{-1}$. The diagonal matrix S contains the singular values – these are identical to the non-negative part of the spectrum of an equivalent hopping problem of *canonical* fermions with hopping energies M_{jk} .
3. We obtain the M' matrix of a particular two-flux sector, defined by a single sign-flipped bond $\langle ij \rangle$ (equivalent to multiplying a single matrix element in M by -1). Now we also perform the SVD for the matrix M' and obtain corresponding U' and V' matrices as well as the singular values $\epsilon_m^{(2)}$. We denote the matter-fermion ground state in this two-flux sector by $|\lambda_0\rangle$ and the canonical fermions describing the corresponding excitations [analogous to those in Eq. (S5)] by \hat{b}_m .
4. We define the matrix

$$X = \frac{1}{2} (U'^T U + V'^T V) \quad (\text{S11})$$

and compute its determinant and its inverse, $\det X$ and X^{-1} , respectively.

5. For an intermediate state with a single matter-fermion excitation, $|\lambda_m\rangle = \hat{b}_m^{\dagger} |\lambda_0\rangle$, matrix elements for \hat{c} operators on the A and B sublattices are obtained as

$$\langle M_0 | \hat{c}_{A,i} | \lambda_m \rangle = \sqrt{|\det X|} (UX^{-1})_{i,m}, \quad (\text{S12})$$

$$\langle \lambda_m | \hat{c}_{B,j} | M_0 \rangle = i \sqrt{|\det X|} (VX^{-1})_{j,m}. \quad (\text{S13})$$

6. Eventually we calculate the correlators (S9) and (S10), with the ground state energy of the flux-free sector E_0 and with the one-particle energies of the considered two-flux sector, with

$$E_{\lambda_m} = E_0^{(2)} + 2\epsilon_m^{(2)} = - \sum_{m'=1}^N \epsilon_{m'}^{(2)} + 2\epsilon_m^{(2)}. \quad (\text{S14})$$

III. FINITE-SIZE AND BOUNDARY EFFECTS

The displacement pattern as described by Eq. (3) is incompatible with periodic boundary conditions, such that open boundaries need to be employed. Then, the pseudo-magnetic field in a finite-size system as in Fig. 1 is not perfectly homogeneous. In addition, low-energy edge states occur. As a result, the clearest Landau-level

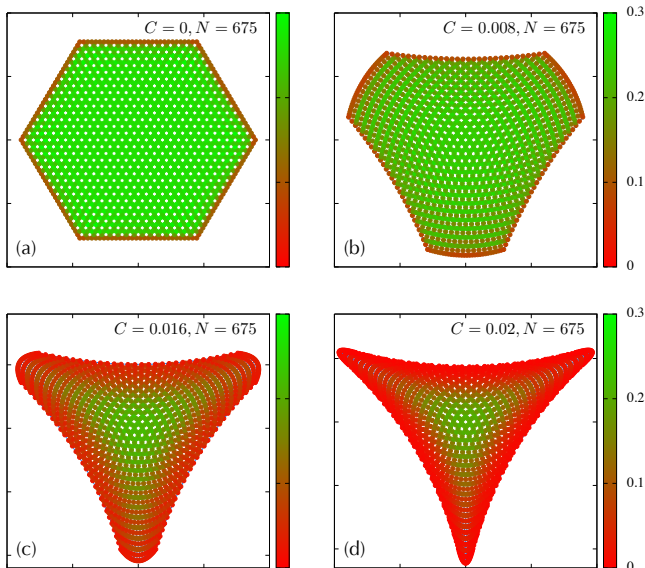


FIG. S2: Local flux gap Δ_{ij}/J . The four panels correspond to different values of C : (a) $C = 0$, (b) $C = 0.008$, (c) $C = 0.016$, and (d) $C = 0.02$. The sample contains $2N = 1350$ lattice sites.

signatures are obtained in the LDOS in the center of the system. This has been discussed in detail for graphene⁵, and our LDOS results including finite-size effects are similar to that in Ref. 5.

A. Edge states

While our system displays edge states at its zigzag edges, these are not topologically protected and do not energetically connect different Landau levels – the latter can be clearly seen in our LDOS results for large values of strain C (not shown). This is consistent with the fact that the strained system remains time-reversal invariant and hence is characterized by a vanishing Chern number.

B. Flux gap for inhomogeneous couplings

For the homogeneous isotropic Kitaev model the flux gap, *i.e.*, the energy difference between the matter-fermion ground states in the two-flux and zero-flux sectors, is given by $\Delta = 0.26J$ in the thermodynamic limit¹. Note that the lowest-energy two-flux states are those with the two fluxes being located in adjacent plaquettes.

Importantly, for a finite-size system with open boundaries the flux gap depends on the spatial position of the flux pair. This requires to introduce a *local* flux gap Δ_{ij} where ij refers to the bond with $u_{ij} = -1$ adjacent to the fluxes. It is this local gap Δ_{ij} which represents the lower energy bound for the intermediate state $|\lambda\rangle$ in the spin correlator $S_{ij}^{\alpha\alpha}(\omega)$.

In Fig. S2 we show Δ_{ij} for different values of the strain C . Clearly, small and moderate values of C lead to an essentially homogeneous gap in the interior of the system and a reduced gap near the edges only. In contrast, for large C the gap profile becomes rather inhomogeneous, with a pronounced maximum in the middle. This can be easily understood: The strongly elongated bonds near the edges correspond to a reduced exchange coupling, and the energy cost of flipping a bond in such a plaquette is small.

C. Local vs. zero-momentum spin correlations

Given the inhomogeneous character of the system, with both the pseudo-magnetic field and the flux gap being approximately homogeneous in the interior only, one has to distinguish measurements in position and momentum space. Momentum-space spin correlations are probed by the dynamic structure factor $S(\vec{q}, \omega)$. For real-space measurements it is convenient to introduce a bond-local response function,

$$S_{\langle ij \rangle}(\omega) = S_{ii}^{\alpha\alpha}(\omega) + S_{jj}^{\alpha\alpha}(\omega) + 2S_{ij}^{\alpha\alpha}(\omega) \quad (\text{S15})$$

with $\alpha = \alpha_{ij}$. The structure factor is related to these local correlators by $\sum_{\alpha} S^{\alpha\alpha}(\vec{q} = 0, \omega) = 1/N \sum_{\langle ij \rangle} S_{\langle ij \rangle}(\omega)$ where the sum $\langle ij \rangle$ is over all lattice bonds.

The plots of Fig. 2 in the main paper display local observables in the center of the system where the Landau-level signatures are clearest – here isolated bound-state peaks are seen in $S_{\langle ij \rangle}(\omega)$. Importantly, the condition of locality for the measurement can be relaxed: In Fig. S3 we show approximants to $(1/3) \sum_{\alpha} S^{\alpha\alpha}(\vec{q} = 0, \omega)$, defined as the sum of all correlators inside a circle of radius R in the interior of the sample:

$$S_R(\omega) = \frac{1}{N'} \sum_{\langle ij \rangle}^{r_i, r_j < R} S_{\langle ij \rangle}(\omega) \quad (\text{S16})$$

where N' the number of bonds inside this circle. For small R , Fig. S3(a), the result for S_R resembles the single-bond result. Increasing R leads to a smearing of the bound-state peaks – this smearing primarily originates from the inhomogeneities in the flux gap. Importantly, the bound-state peaks characteristic of the Landau-level structure are still clearly visible for R values where the circle covers a sizeable fraction of the sample, 14% in Fig. S3(c). This shows that neutron-scattering measurements can detect the peak structure by measuring $S(\vec{q}, \omega)$ provided that the neutron beam is smaller than the sample size, such that the outer parts of the sample are not included in the probe.

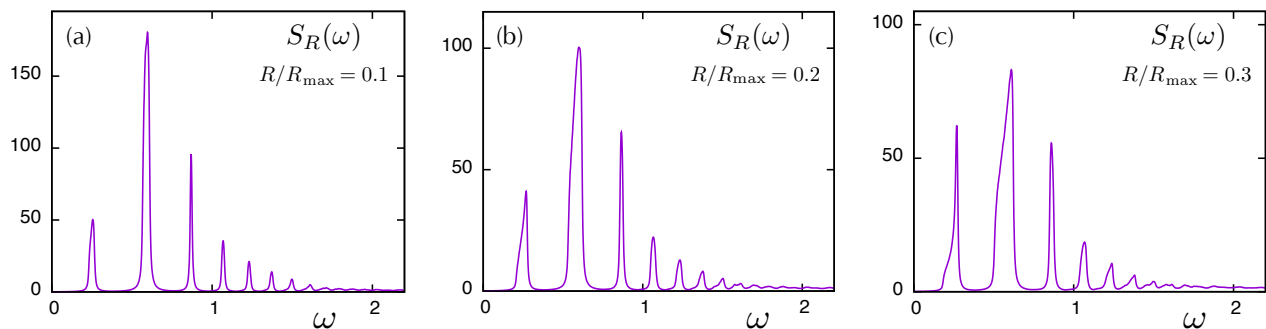


FIG. S3: Correlators $S_R(\omega)$ (S16) – representing a finite-area approximant to $S(\vec{q}=0, \omega)$ – for (a) $R/R_{\max} = 0.1$, featuring essentially the same peak structure as $S_{(ij)}(\omega)$ in Fig. 2(i), (b) $R/R_{\max} = 0.2$, with visible broadening of the bound-state peak due to inhomogeneities, and (c) $R/R_{\max} = 0.3$. The system parameters are $2N = 15\,000$, $C = 0.004$, and R_{\max} is the radius of the smallest circle enclosing the entire flake (in unstrained coordinates). The Lorentzian broadening is $\gamma/J = 0.005$.

D. Thermodynamic limit

The displacement pattern used to generate the pseudo-magnetic field, Eq. (3), cannot be extended to an infinitely large system, simply because bond lengths become negative. In other words, the thermodynamic limit of infinite linear size, $L/a_0 \rightarrow \infty$, cannot be taken at fixed \bar{C} . We also note that, with increasing system size, the linearization in Eq. (4) becomes invalid, which is eventually signalled by negative exchange couplings at the boundary (for the strain values used in this paper, all couplings remain positive). Together, this raises the question whether there exists a well-defined limit where finite-size effects can be made small.

An interesting route is to take the combined limit $L/a_0 \rightarrow \infty$ and $\bar{C} \rightarrow 0$, keeping $\bar{C}L/a_0$ (as well as the magnetoelastic factor β) fixed. In this limit, the pseudo-magnetic field scales to zero as $L/a_0 \rightarrow \infty$, and with it the energetic spacing of the pseudo-Landau levels. As the ratio of system size and magnetic length is kept fixed, we speculate that the system approaches a scaling limit with well-defined Landau levels – this will be investigated in future work.

E. Spin correlations at finite temperature

For an orbital magnetic field applied to graphene, the lowest Landau level (LLL) is located at exactly zero energy. For the present case of the strained Kitaev model, the LLL being at zero energy implies a highly degenerate many-body ground state. Notably, this degeneracy is lifted by finite-size effects – all our mode energies ϵ_m are positive.

For practical reasons, we evaluate the expectation value $\langle \dots \rangle$ in the spin correlator, $S_{ij}^{\alpha\beta}$ in Eq. (5), with the unique finite-system ground state $|M_0\rangle$, corresponding to strictly $T = 0$. Importantly, our conclusions apply unchanged if $S_{ij}^{\alpha\beta}$ is calculated instead using a thermal aver-

age over the low-energy many-body states, i.e., at small finite temperature $T \ll \varepsilon_1$ where ε_1 is the energy of the first finite-energy Landau level. The argument proceeds as follows: The relevant many-body initial states $|M\rangle$ involve any number of matter Majorana excitations from the LLL – this precludes a full numerical evaluation of $S_{ij}^{\alpha\beta}$ at finite T . Importantly, for large systems, sizeable matrix elements $\langle \lambda | \hat{c}_j | M \rangle$ are only obtained if the intermediate state contains, in addition to the excitation effectively created by \hat{c}_j , the *same* excitations as the initial state $|M\rangle$. This has been demonstrated in Ref. 3 where the effect of the ground-state fermion-parity condition^{3,4} on the spin structure factor has been examined: It was found that the two-particle continuum, obtained by starting from an initial state with one excited fermion, is virtually indistinguishable from the one-particle continuum, obtained by starting from an excitation-free initial state. More precisely, the differences between the two results for $S_{ij}^{\alpha\beta}$ scale with the inverse system size, the reason being that the wavefunctions of the additional excitations are spatially extended. Generalized to our system, this implies that all thermal contributions to the low-temperature spin correlator will have essentially the same peak structure, arising from the bound states between the Majorana Landau levels. While small finite temperatures will cause both small broadening and a small weight redistribution, the peak structure in $S(\omega)$ shown in Fig. 2 can be expected to be robust.

IV. PSEUDO-LANDAU LEVELS AND BOUND STATES

As emphasized in the paper, sufficiently large strain induces pseudo-Landau levels in the matter Majorana sector of the Kitaev model. At the same time, the dynamic spin correlator $S_{(ij)}(\omega)$ shows sharp δ peaks. Interestingly, these peaks (with the exception of the lowest one which can be attributed to the LLL in the two-flux sector) do *not* directly arise from the Landau levels.

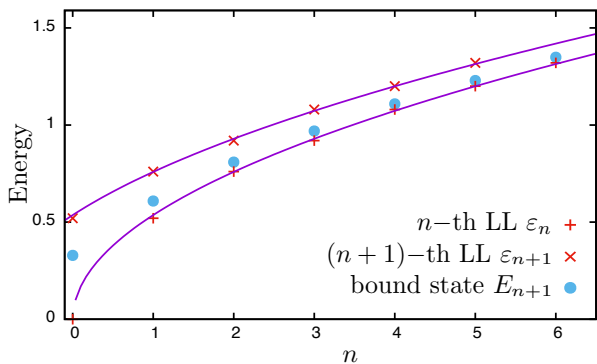


FIG. S4: Energy positions of the Landau levels ε_n as observed in the matter-fermion LDOS of the flux-free sector, shown together with the bound-state energies E_n in the two-flux sector; the E_n are identical to the peak positions in the correlator $S_{\langle ij \rangle}(\omega)$ with the local flux gap Δ_{ij} subtracted [except for the lowest peak which originates from the LLL; hence our numbering for E_n starts with $n = 1$]. The data correspond to that of Fig. 2(g,i) of the main paper, with $2N = 15000$ and $C = 0.004$. The lines are fits of ε_n to a \sqrt{n} dependence; both ε_n and ε_{n+1} are shown for visualization purposes such that the two red data points for each n mark the Landau-level gap.

Instead the measurement dynamically generates an impurity leading to one localized bound state, causing a high-intensity peak in $S_{\langle ij \rangle}(\omega)$, in each of the Landau-level gaps. Given that higher Landau levels tend to be smeared (because the analogy between strain and magnetic field is restricted to the low-energy limit), the spin correlator shows a much sharper peak structure than the matter-fermion DOS itself.

A. Energy scaling

In Fig. S4 we show the energetic positions of the bound-state peaks in $S_{\langle ij \rangle}(\omega)$, with the local flux gap Δ_{ij} subtracted, and compare them to the energies of the Landau levels found in the matter-fermion LDOS of

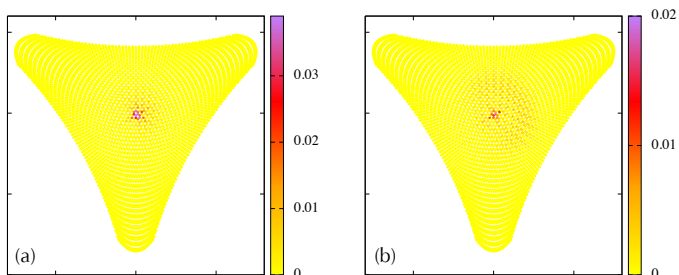


FIG. S5: Wavefunctions of the first two in-gap bound states in the two-flux sector for a system with $2N = 5400$ spins and strain $C = 0.0078$ where the flux pair has been created in the center. (a) First in-gap state with energy $E_{n=1} \approx 0.44 J$. (b) Second in-gap state at $E_{n=2} \approx 0.86 J$.

the flux-free system. The plot shows that the energies of the pseudo-Landau levels fit the energy dependence $\varepsilon_n \propto \sqrt{B|n|}$ known for graphene Landau levels where B encodes magnetic field strength⁶. The bound-state energies track this dependence, approaching the lower edge of the respective gap with increasing n . Hence, the observation of a series peaks in $S_{\langle ij \rangle}(\omega)$ with a \sqrt{n} energy dependence (after subtracting a constant corresponding to Δ_{ij}) can be taken as a unique signature of the Landau-level structure.

B. Bound-state wavefunctions

In Fig. S5 we illustrate the nature of the probe-induced bound states in the two-flux sector, by plotting the probability distribution of eigenmode m for A and B sites given by

$$w_{A,i}^m = U_{mi}^2/2, \quad w_{B,j}^m = V_{mj}^2/2. \quad (\text{S17})$$

The bound-state eigenmodes are highly localized near the flipped bond (which is taken to be in the center of the sample), which we have checked by computing the inverse participation ratio for these modes. The localization length increasing with increasing n , which is a simple result of the decreasing gap magnitude.

C. Bound states and topology

A recent paper⁷ has proposed an interesting connection between topological states and local impurity physics, namely that the impurity-induced local in-gap Green's function can be used as diagnostic tool for topology. For time-reversal-invariant \mathbb{Z}_2 topological insulators in two

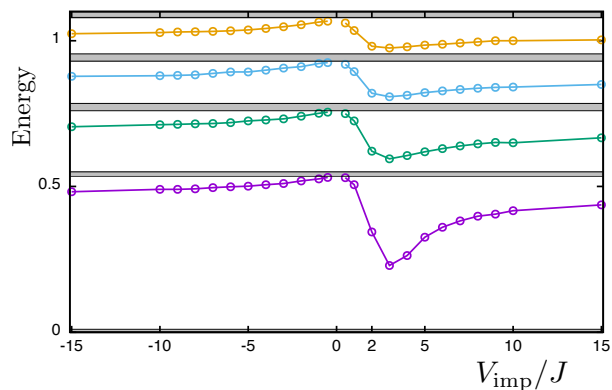


FIG. S6: Energy positions E_n of the bound states caused by a bond impurity as a function of the impurity strength V_{imp} . Note that $V_{\text{imp}} = 0$ is the clean case and $V_{\text{imp}} = 2J_{ij}$ corresponds to a flipped bond (“two-flux sector”). The data corresponds to $N = 7500$ and $C = 0.004$; the grey horizontal lines represent the energies of the pseudo-Landau levels.

space dimensions a local impurity always causes an in-gap bound state. This is because the real part of the local Green's function diverges at the lower edge of the upper band with opposite sign compared to the upper edge of the lower band. This guarantees the presence of an in-gap bound state. It was further shown that a topologically trivial insulator does not generally possess such in-gap bound states (but may do so in a finite interval of impurity strengths).

As our analysis has revealed the creation of localized in-gap states due to bond impurities, the latter representing a pair of Z_2 fluxes, we adapt the idea of Ref. 7 to our setting. We consider a bond impurity of general

strength, $\hat{V} = -iV_{\text{imp}}\hat{c}_i\hat{c}_j$, in a honeycomb-lattice Majorana hopping problem subject to triaxial strain. While the impurity value $V_{\text{imp}} = -2$ (measured in units of J_{ij}) corresponds to a flipped bond, *i.e.*, a two-flux sector, here we consider arbitrary values of $V_{\text{imp}} \in [-15, 15]$, with the clean case corresponding to $V_{\text{imp}} = 0$. As shown in Fig. S6, we find that bond impurities of any strength induce bound states between the Landau levels (except for the immediate vicinity of $V_{\text{imp}} = 0$ where any bound state must occur close to a gap edge and is thus hard to detect in a finite-size system). Hence, the criterion of Ref. 7 suggests that the matter-fermion sector of the strained Kitaev model displays non-trivial topology.

¹ A. Kitaev, Ann. Phys. (N.Y.) **321**, 2 (2006).

² J. Knolle, D. L. Kovrizhin, J. T. Chalker, and R. Moessner, Phys. Rev. Lett. **112**, 207203 (2014).

³ F. Zschocke and M. Vojta, Phys. Rev. B **92**, 014403 (2015).

⁴ F. L. Pedrocchi, S. Chesi, and D. Loss, Phys. Rev. B **84**, 165414 (2011).

⁵ M. Neek-Amal, L. Covaci, K. Shakouri, and F. M. Peeters,

Phys. Rev. B **88**, 115428 (2013).

⁶ A. J. M. Giesbers, U. Zeitler, M. I. Katsnelson, L. A. Ponomarenko, T. M. Mohiuddin, and J. C. Maan, Phys. Rev. Lett. **99**, 206803 (2007).

⁷ R.-J. Slager, L. Rademaker, J. Zaanen, and L. Balents, Phys. Rev. B **92**, 085126 (2015).